Available online at www.sciencedirect.com
SCIENCE DIRECT®
Composites Science and Technology 66 (2006) 137–150
COMPOSITES SCIENCE AND TECHNOLOGY
www.elsevier.com/locate/compscitech

A direct micromechanics method for analysis of failure initiation of plain weave textile composites

Ryan L. Karkkainen [1], Bhavani V. Sankar *

Mechanical and Aerospace Engineering Department, University of Florida, 231 MAE-A Building, P.O. Box 116250, Gainesville, FL, 32611-6250, United States

Received 11 November 2004; received in revised form 5 April 2005; accepted 19 May 2005
Available online 14 July 2005

Abstract

A micromechanical analysis of the representative volume element (RVE) of a plain weave textile composite has been performed using the finite element method. Stress gradient effects are investigated, and it is assumed that the stress state is not uniform across the RVE. This is unlike most stiffness and strength models, which start with the premise that an RVE is subjected to a uniform stress or strain. For textile geometries, non-uniform stress considerations are important, as the size of a textile RVE will typically be several orders of magnitude larger than that of a unidirectional RVE, for which many analysis techniques are developed. The stress state is defined in terms of the well-known laminate theory force and moment resultants $[N]$ and $[M]$. Structural stiffness coefficients analogous to the $[A]$, $[B]$, $[D]$ matrices are defined, and these are computed directly using the direct micromechanics method (DMM), rather than making estimations based upon homogenized properties. Failure envelopes for a plain-weave textile composite have been constructed. Transverse failure of the fiber tow was the dominant mode of initial failure. The DMM failure envelope compared closely to the Tsai-Wu failure theory, but was more conservative in some areas.

Keywords: A. Textile Composites; B. Strength; C. Finite element analysis

1. Introduction

Current failure theories are generally developed for unidirectional composites and do not capture the unique characteristics of textile composites. Though these theories may to some extent be applied in an adapted form to the analysis of textile composites, many inherent simplifying assumptions will no longer apply, and in general such techniques will not be suitable to the increased complexity intrinsic to textile geometry. Even at the micro scale, textile composites maintain a relatively complicated microstructure. Even under simple loading conditions, a textile microstress state will be shown to be quite complex, and elastic constants are non-uniform due to the waviness of a woven fiber tow. Laminate analysis, property homogenization, and other common approaches will no longer apply. Thus, current designs of textile structures will not be optimized for maximum damage resistance and light-weight.

Conventional micromechanical models for textile composites assume that the state of stress is uniform over a distance comparable to the dimensions of the representative volume element (RVE). However, due to complexity of the weave geometry, the size of the RVE in textile composites can be large compared to structural dimensions. In such cases, severe non-uniformities in the stress state will exist, and conventional models may fail. Such stress gradients also exist when the load is applied

* Corresponding author. Tel.: +1 352 392 6749; fax: +1 352 392 7303.
E-mail addresses: rkarkkai@ufl.edu (R.L. Karkkainen), sankar@ufl.edu (B.V. Sankar).
[1] Graduate Student. Tel.: +1 352 846 3027; fax: +1 352 846 3028.

0266-3538/$ - see front matter © 2005 Elsevier Ltd. All rights reserved.
doi:10.1016/j.compscitech.2005.05.018

Nomenclature

σ^{M}	macroscopic level stress	z	distance from RVE midplane in the height direction
σ^{e}	element level stress	E	Young's modulus
σ_i	normal stress in the i direction	G	shear stiffness
τ_{xy}	shear stress in the x–y plane	v	Poisson ratio
a	RVE width	V_f	fiber volume fraction
b	RVE depth	V^{e}	element volume
c	RVE height	u	displacement
N_i	force resultant in the i direction	H_{ij}	deformation gradients
N_{xy}	shear force resultant in the x–y plane	X_T	maximum force resultant before failure in tension in the x-direction
M_i	moment resultant in the i direction	X_C	maximum force resultant before failure in compression in the x-direction
M_{xy}	torque resultant in the x–y plane	Y_T	maximum force resultant before failure in tension in the y-direction
ε_i	normal strain in the i direction	Y_C	maximum force resultant before failure in compression in the y-direction
γ_{xy}	shear strain in the x–y plane	S	maximum in-plane shear force resultant before failure
κ_i	curvature in the i direction		
κ_{xy}	twist in the x–y direction		
$[A]$	in-plane stiffness matrix		
$[B]$	strain-curvature coupling matrix		
$[D]$	flexural stiffness matrix		

over a very small region, as in static contact or foreign object impact loading, and when there are stress concentration effects such as open holes in a structure.

Although micromechanical models have been successfully employed in predicting thermo-elastic constants of fiber-reinforced composite materials, their use for strength prediction in multiaxial loading conditions is not practical, as computational analysis must be performed in each loading case. Thus, phenomenological failure criteria are still the predominant choice for design in industry. There are three major types of engineering failure criteria for unidirectional composite materials: maximum stress criterion, maximum strain criterion, and quadratic interaction criterion, such as the Tsai-Hill and Tsai-Wu failure theories [1].

Most of the micromechanical modeling work done thus far have focused on predicting thermo-mechanical properties [2–5]. To facilitate the use of textile composites in lightweight structures, it is required to have a lucid understanding of failure mechanisms, and design engineers must have an accurate and practical model for prediction of failure stress. Most of the current analytical and numerical methodologies developed to characterize textile composites [6–13] assume that the textile is a homogeneous material at the macroscopic scale.

Finite element analysis of initial failure of a plain weave composite [9] has shown that failure due to inter-tow normal stresses are the predominant mode of failure, and there is generally little or no damage volume of the bulk matrix between tows. This work is extended to a thorough investigation of progressive failure analysis under axial extension using several different property knockdown schemes. This has shown stiffness losses on the order of 40% after initial failure. More recently this work has been extended to include the capability for more detailed stress fields in the RVE under investigation [14], and techniques have been developed to minimize required computation times by employing boundary conditions based on thorough exploitation of symmetry and periodicity of RVE geometry [15].

The Binary Model [16,17] allows for quick and efficient finite element analysis of any textile weave of interest. Fiber tows are modeled simply and reasonably as embedded 1-D line elements within the bulk matrix. This method has been shown to provide for accurate prediction of stiffness properties. Further, it is robust and readily adaptable to provide insight into effects of alteration of parameters such as tow waviness, tow misalignment, varying weave architectures, etc. This technique does not yield a detailed map of RVE stress fields or allow for cross-sectional variation of tow geometry, as the fiber tow is simulated as a 1-D line element with representative material properties. Thus, some micro-level detail is lost to provide for computational efficiency and macro-level representation.

The Mosaic Model and its adaptations [6,18,19] represent a textile composite RVE as a collection of homogenized blocks, each with unidirectional composite or matrix properties. These blocks are then assembled to represent the weave geometry under consideration. In this way, classical laminate plate theory can be used to determine the global stiffness matrix of the RVE. For macroscopically homogeneous load cases, good agreement has been shown with experimental data, including three-dimensional weave geometries.

Effective prediction of compressive strength of braided textile composites using a detailed FEM micromechanical model has been performed [20], which shows good comparison to experimental results in a parallel study [21]. A detailed 3D solid model was formed to exactly model a 2D triaxially braided composite RVE. Biaxial loading is considered in both the experimental and computational analyses. Buckling analysis has been performed, and the effects of tow waviness and microarchitecture on the compressive strength are shown.

For uniaxially loaded textile composites, consistent but optimistic strength estimates have been made by comparing the strength of fiber tows with the predicted stresses in the fiber yarns that are aligned with the loading axis [22–24]. The off-axis tows are given little consideration, without much effect on the outcome, as they play little part in such uniaxial loading cases. Multi-axial loading presents an obvious escalation in modeling complexity. The failure envelope for combined transverse tension and in-plane shear has been presented as an ellipse [25], according to quadratic strength rules developed for unidirectional composites. Further, proposals for multiaxial loadings submit that axial strain in the textile geometry should be compared to a critical value of tow strain, analogous to a first-ply failure criterion for unidirectional composites [26].

A previous study by the authors [27] extended a method, known as the direct micromechanics method (DMM) [28], to develop failure envelopes for a plain-weave textile composite under plane stress in terms of applied macroscopic stresses. In this study, it was assumed that the state of stress is uniform across the RVE. The micro scale stresses within the RVE were computed using finite element methods. The relation between the average macrostress and macrostrains provide the constitutive relations for the idealized homogeneous material. The microstresses are used to predict the failure of the yarn or matrix, which in turn translates to failure of the textile composite.

In the current paper, micromechanical finite element analysis is performed to determine the constitutive relations and failure envelope for a plain-weave graphite/epoxy textile composite. The model is based upon the analysis of an RVE, which is subjected to force and moment resultants of classical laminate theory. Thus, there is no assumption about the uniformity of an applied load or strain, as any load can be represented by a combination of force and moment resultants. The microscale stresses within the RVE are computed using the finite element method. The relation between the average macrostress and macrostrains provide the constitutive relations for the material. Thus constitutive characterization matrices $[A]$, $[B]$, $[D]$ are found directly from micromechanics. The microstresses are also used to predict the failure of the yarn or matrix, which in turn translates to failure of the textile composite. Using the DMM, the failure envelope is developed for in-plane force resultants, with and without applied moment resultants. No currently accepted failure criteria exist that may be used explicitly for the analysis of textile composites. Thus, the methods and results employed herein are used to develop phenomenological failure criteria for textile composites. The results are compared to conventional failure envelopes that are not specifically developed for the analysis of textile composites, as a basis for evaluation.

2. Methods

2.1. Finite element micromechanical method

In the current study, stress gradient effects are investigated, and it is assumed that the stress state is not uniform across the RVE. This represents an extension of the micromechanical models used to predict the strength of textile composites [27–31]. The stress state is defined in terms of the well-known laminate theory load matrices $[N]$ and $[M]$, i.e., force and moment resultants. Furthermore, structural stiffness coefficients analogous to the $[A]$, $[B]$, $[D]$ matrices are defined. In this approach, these structural stiffness coefficients are computed directly from the micromechanical models, rather than making estimations based upon the homogeneous Young's modulus and plate thickness, i.e., individual unit strains and unit curvatures can be applied to the micromechanical finite element model, and the resulting deformations are used to define the stiffness coefficient matrices. Conventional models essentially neglect the presence of $[M]$ terms that result from non-uniformity or gradients in applied force resultants, thus assuming a uniform stress state for which only the $[N]$ matrix is populated. The additional analysis of the $[M]$ term includes information about the distribution, or gradient, of a non-uniform load. This can greatly increase the ability of a failure model to accurately predict failure for load cases in which such effects may well be predominant, such as in thin plates, concentrated loading, or impact loading.

The significance of including the analysis of moment terms is further illustrated in Fig. 1. The moment term describes the *distribution*, not only the *magnitude*, of applied loading. Depending on the stress state of an RVE, an analysis incorporating stress gradient effects and inclusion of the consideration of applied moment could be of critical importance. In Fig. 1(a), the force resultant (N) is non-zero, but the uniform loading results in zero moment resultant (M). However, in load cases such as Fig. 1(b) and (c), the non-uniformity of applied loading leads directly to an appreciable moment term, which must be included in the analysis. In fact, in some cases it is possible that the net force resultant is zero while

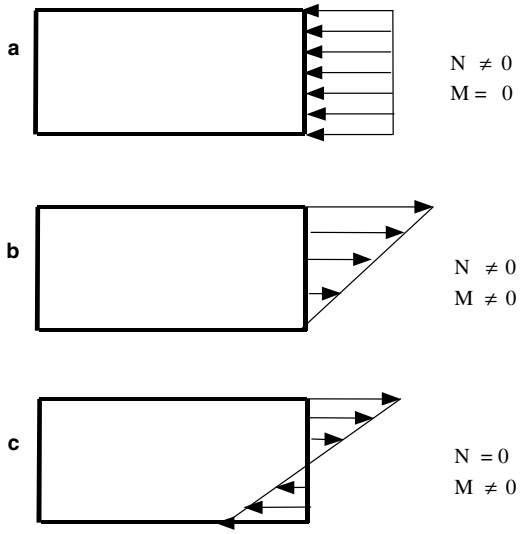

Fig. 1. Example load cases to illustrate the importance of including moment terms in the analysis of a textile RVE. Distributed loads across the large dimensions of a textile RVE will produce bending moments that must be incorporated into stiffness and strength prediction.

the effective moment resultant is non-zero, in which case conventional analysis techniques cannot be employed.

The present micromechanical analysis of a plain-weave textile composite is performed by analyzing the representative volume element (RVE) using the finite element method. A weave-architecture has been selected and this RVE is detailed in Table 1 and also in Fig. 2. This architecture was chosen from a literature source [32] that provided a complete and detailed description of the needed geometrical parameters, such as those shown in Table 1. Given parameters are representative of microarchitectures as experimentally observed via SEM or standard microscope. Total fiber volume fraction, given these dimensions, will be 25%, incorporating

Table 1
RVE dimensions

Dimension	*a*, *b*	*c*	*p*	*t*	*w*
Length (mm)	1.68	0.254	0.84	0.066	0.70

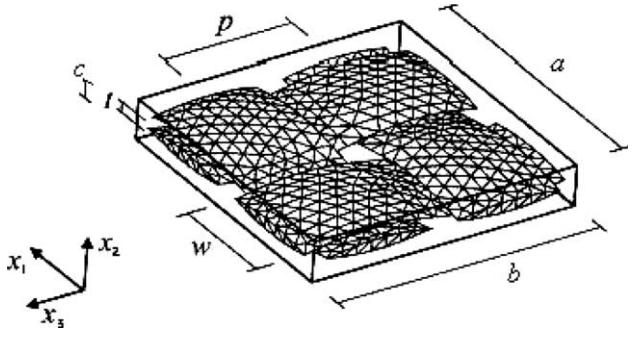

Fig. 2. RVE geometry of a plain weave textile composite.

the fact that the resin-impregnated tow itself has a fiber volume fraction of 65% (this is calculated directly from ABAQUS software, which yields element volumes as outputs, thus the volume of all matrix elements can be compared to the volume of all tow elements). Though this volume fraction may seem low for structural uses, it can be representative of many significant low-load, impact-resistant applications, such as automotive light-weight body panels. It should be noted that a number of parameters are required to exactly specify the textile geometry. These specifications will have a significant effect on micromechanical modeling. Consequently, care should be taken when comparing the results of various studies that the textile geometries under comparison are truly equivalent.

In order to evaluate the stiffness and strength properties of the textile weave under consideration, the DMM is essentially employed as an analytical "laboratory" that quickly and effectively replaces physical testing and experimental procedures. Though experimental verification always provides a baseline of veracity to FEM analysis, this procedure effectively overcomes the limitations of physical apparatus. And furthermore, as will be shown later, this allows for a dense population of analysis points, i.e., a failure envelope may be quickly and fully constructed with a large number of data points, and there is no need for interpolation of limited discrete experimental data points. Also, results achieved from the DMM are completely three-dimensional stress or strain fields, i.e., the results can be visualized throughout the thickness of the specimen. This overcomes the limitations inherent to physical application of experimental stress analysis techniques, which are labor-intensive and generally limited to surface visualizations.

Specification of relative displacements on opposite faces of the RVE can represent any general macro deformation under investigation. Displacements are applied using periodic boundary conditions. The periodic displacement boundary conditions isolate the mechanical effects of application of unit strains or curvatures, and ensure the repeatability of deformations. Thus, the RVE is not only repeatable as a representative geometry, but is also mechanically repeatable in that each RVE has an identical response to strains and curvatures regardless of the location of that RVE in a textile plate or component, for example:

$$\left.\frac{\partial u_i}{\partial x_j}\right|_x = \left.\frac{\partial u_i}{\partial x_j}\right|_{x+a}, \quad \left.\frac{\partial^2 w}{\partial x^2}\right|_x = \left.\frac{\partial^2 w}{\partial x^2}\right|_{x+a}. \tag{1}$$

To ensure continuity of microstresses and compatibility of displacements across an RVE, periodic traction and displacement boundary conditions must be employed. A macroscopically homogeneous deformation can be represented as:

$$u_i^{\mathrm{M}} = H_{ij}x_j \quad i,j = 1,2,3, \tag{2}$$

e.g., $u_i(a,x_2,x_3) - u_i(0,x_2,x_3) = H_{i1}a,$
$u_i(x_1,b,x_3) - u_i(x_1,0,x_3) = H_{i2}b.$

The derivation of the periodic boundary condition for unit curvature is presented below, and further examples are presented in the appendix.

The periodic displacement boundary condition corresponding to unit curvature along the x-axis (κ_x) will be derived. All other curvatures will be zero. Curvatures are defined as follows:

$$\kappa_x = -\frac{\partial^2 w}{\partial x^2} = 1, \quad \kappa_y = -\frac{\partial^2 w}{\partial y^2} = 0, \quad \kappa_{xy} = -\frac{\partial^2 w}{\partial x \partial y} = 0. \tag{3}$$

The periodic displacement boundary condition will be derived from the definition of curvature along the x-axis (κ_x). Integrating once with respect to x yields:

$$-\frac{\partial w}{\partial x} = x + f(y), \tag{4}$$

where $f(y)$ is an arbitrary function of y. Differentiation of this expression with respect to y, together with the requirement that κ_{xy} is set as zero, indicates that:

$$\kappa_{xy} = -\frac{\partial^2 w}{\partial x \partial y} = f'(y) = 0. \tag{5}$$

Due to the above expression, $f(y)$ must therefore be a constant, since $\kappa_{xy} = 0$. Furthermore, this constant must be zero due to the specification that slope at the origin is zero, i.e., $\frac{\partial w}{\partial x}|_{x=0} = 0$. Next, Eq. (4) is integrated with respect to x, giving rise to the following expression and an arbitrary function $h(y)$:

$$-w = \frac{x^2}{2} + h(y). \tag{6}$$

Now coordinate values for opposite faces of the RVE (see Fig. 2) may be substituted into Eq. (6):

$$\begin{aligned} w(a,y,z) &= -\frac{1}{2}a^2 + h(y), \\ w(0,y,z) &= h(y). \end{aligned} \tag{7}$$

These are then subtracted from each other, eliminating the unknown $h(y)$, and effectively prescribing the relative displacement on opposite faces that can be used to apply unit curvature,

$$w(a,y,z) - w(0,y,z) = -\frac{1}{2}a^2. \tag{8}$$

However, a further boundary condition is required to remove the transverse shear forces that will be present due to the application of this displacement. In this way, the mechanical effect of curvature is isolated. Thus the requirement is that transverse shear strain is zero, which is defined as:

$$\gamma_{zx} = \frac{\partial u}{\partial z} + \frac{\partial w}{\partial x} = 0. \tag{9}$$

This can be rearranged as below, and the value of slope $\frac{\partial w}{\partial x}$ is known from Eq. (4) above (where the arbitrary function has been shown to be zero):

$$\frac{\partial u}{\partial z} = -\frac{\partial w}{\partial x} = x. \tag{10}$$

Similar to the above procedure, this expression can then be integrated with respect to z, evaluated with coordinate values of opposite faces, which are then subtracted from each other to specify the relative displacement that must be prescribed:

$$u = zx + c, \tag{11}$$

$$u(a,y,z) - u(0,y,z) = za. \tag{12}$$

Thus, the periodic boundary conditions as shown in Eqs. (8) and (12) must be simultaneously applied to isolate the effects of an applied unit-curvature, as seen in Table 2.

In order to satisfy equilibrium, traction boundary conditions are applied to ensure equal and opposite forces on opposite faces of the RVE. The traction boundary conditions for traction forces on the lateral faces of the RVE are:

$$\begin{aligned} F_i(a,y,z) &= -F_i(0,y,z), \\ F_i(x,b,z) &= -F_i(x,0,z), \\ F_i(x,y,c) &= -F_i(x,y,0). \end{aligned} \tag{13}$$

In DMM, the RVE is subjected to macroscopic force and moment resultants, which are related to macroscopic strain and curvature according to:

$$\begin{Bmatrix} [N] \\ [M] \end{Bmatrix} = \begin{bmatrix} [A] & [B] \\ [B] & [D] \end{bmatrix} \begin{Bmatrix} [\varepsilon] \\ [\kappa] \end{Bmatrix}. \tag{14}$$

Table 2
Periodic displacement boundary conditions

		$u(a,y) - u(0,y)$	$v(a,y) - v(0,y)$	$W(a,y) - W(0,y)$	$u(x,b) - u(x,0)$	$v(x,b) - v(x,0)$	$w(x,b) - w(x,0)$
1	$\varepsilon_x^M = 1$	a	0	0	0	0	0
2	$\varepsilon_y^M = 1$	0	0	0	0	b	0
3	$\gamma_{xy}^M = 1$	0	$a/2$	0	$b/2$	0	0
4	$\kappa_x^M = 1$	az	0	$-a^2/2$	0	0	0
5	$\kappa_y^M = 1$	0	0	0	0	bz	$-b^2/2$
6	$\kappa_{xy}^M = 1$	0	$az/2$	$-ay/2$	$bz/2$	0	$-bx/2$

Thus, the constitutive matrices must be evaluated to determine this correlation. Once this has been determined, a macroscopic deformation can be applied using an FEM code. In this way, the FEM results for stress in each element yield the microstresses resulting from an applied force or moment resultant.

The RVE is subjected to independent macroscopic unit deformations in order to evaluate the stiffness matrices of Eq. (14). In each of the six cases shown in Table 2 below, a single unit strain or a single unit curvature is applied, and all other deformation terms are set to zero, and the appropriate periodic boundary conditions are applied.

The four-node linear tetragonal elements in the commercial ABAQUS™ (Standard) FEM software package were used to model the yarn and matrix for all cases. An *h*-refinement convergence study was performed in which analysis was performed for a progressively finer mesh of four-node linear tetragonal elements. For several reasons, the final mesh chosen employs 68,730 such elements. This refinement is significantly beyond the point of numerical convergence for which output element stresses can be assured to be accurate. This also allows for a mesh that accurately covers the "corners" of an ellipsoidal tow cross-section without sacrificing element quality in such regions. Furthermore, a refined mesh can capture the intricacies of stress contours and stress gradients expected to be seen through the RVE. Note that the shared nodes are employed between each tow and its surrounding interstitial matrix. There are no tow-tow shared nodes, thus tows are allowed to slide over each other. As a final note on the character and quality of mesh employed in this analysis, the following quality assurance metrics are indicated: fewer than 0.1% of elements have an interior angle less than 20°, fewer than 0.3% have an interior angle greater than 120°, and less than 0.2% have an aspect ratio greater than 3 (the average aspect ratio is 1.66).

The FEM results for each element yield the microstresses resulting from an applied macro-level strain and curvature. The corresponding macro-level force and moment resultants in each case can be computed by averaging the microstresses over the entire volume of the RVE:

$$N_{ij} = (1/ab)\sum \sigma^{e}_{ij} V^{e}, \tag{15}$$

$$M_{ij} = (1/ab)\sum z\sigma^{e}_{ij} V^{e}. \tag{16}$$

Thus, the constitutive matrices of Eq. (14) can be found by independently evaluating the six cases shown in Table 2, in tandem with Eqs. (15) and (16). By applying the appropriate displacements according to Table 2 which correspond to a given unit strain or curvature case, the stiffness coefficients in a column corresponding to the non-zero strain can be evaluated directly from the force and moment resultant values as calculated from the finite element micro stresses via Eqs. (4) and (5). Thus the six load cases completely describe the six columns of the $[A]$, $[B]$, $[D]$ matrix.

This information having been determined, one is then able to evaluate the microstress field resulting from general loading cases via the following steps: Step (1) Relate applied force and moment resultants to applied macro strain and curvature via the $[A]$, $[B]$, $[D]$ matrices and Eq. (3), Step (2) Apply this macro strain and curvature to the RVE using an FEM code, and Step (3) The element stresses from FEM results yield the microstress field in the yarn and matrix. The present study assumes there are no residual stresses or pre-stresses in the composite. The significance of residual stresses would depend on the particular cure cycle employed in manufacturing the composite, as well as upon the weave pattern under investigation. For a plain-weave textile, it would be expected that residual pre-stresses would affect the "center point" of the failure envelope, given that: (1) symmetry of microarchitecture would lead to a level of symmetry of residual stresses, and (2) pre-stresses shift, rather than shrink, an existing failure envelope as the applied loads can either add to or be offset by the residual stresses. The magnitude of residual stresses could conceivably reach on the order of 10% of the failure strength.

2.2. Direct micromechanics method for failure analysis

The method described above can be used to predict failure strength by comparing the computed microstresses in each element against failure criteria for the constituent yarn and matrix of the textile composite. Interface failure is not considered in the current study, but will be incorporated into future work. The microstresses in each element can be extrapolated from the preliminary RVE analysis (described above) of each of the six linearly independent macrostrain components. The microstress state for a general applied force or moment resultant is obtained by superposing multiples of the results from the unit macrostrain analysis:

$$\{\sigma^{e}\} = [F^{e}]\begin{Bmatrix} \varepsilon^{M} \\ \kappa^{M} \end{Bmatrix}, \tag{17}$$

where the 6×6 matrix $[F^{e}]$ contains the microstress in each element resulting from the unit strain and curvature analysis. For example, the microstress σ_y in the RVE for $\varepsilon_{x0} = 0.05$ and $\kappa_y = 0.003\ \mathrm{m}^{-1}$ is calculated as $\sigma_y = 0.05F_{21} + 0.003F_{25}$.

Failure is checked on an element-by-element basis, and the failure criterion of each element can be selected appropriately based upon whether it is a yarn or matrix element. It is assumed that the entire textile

composite has failed, even if only one of the yarn or matrix elements has failed. Although this may be considered conservative, it is realistically representative of the initial failure of the composite. It can be thought of by analogy to the first-ply failure of a laminated composite, i.e., the point at which property loss becomes significant, even if remaining material can continue to support applied loading. For the isotropic matrix elements, the maximum principal stress criterion is used to evaluate element failure. For fiber tow elements, the Tsai-Wu failure criterion is used. This criterion is more suitable to the orthotropic nature of the fiber tow, which is essentially a unidirectional composite at the micro level. Microstresses in the yarn are transformed to local coordinates tangent to the path of the yarn and compared to strength coefficients for a unidirectional composite, using the Tsai-Wu criterion.

A flow chart that describes the DMM procedure is shown in Fig. 3. Failure envelopes are generated by first selecting a macrostress state to investigate. Then the macrostrains and curvatures resulting from this applied loading are calculated from Eq. (14). The resulting stress field for the entire RVE is then calculated by Eq. (17), based on the scaled superposition of the results from FEM analysis of the unit load cases shown in Table 2. Failure is then checked in each element against a given failure criterion. This cycle is then repeated while progressively increasing a selected force or moment resultant and holding all others constant until an element level failure criterion is exceeded. If a particular failure criterion is exceeded, the element and the RVE are considered to have failed, which then defines the threshold of the failure envelope at a given point. Thus, failure envelopes for the textile composite can be generated in various force and moment resultant spaces. The scope of the current study considers analysis of in-plane force and moment resultants $[N]$ and $[M]$, though the methods are applicable to any general loading conditions.

2.3. Phenomenological failure criteria

In addition to being used to determine failure of the fiber tow or the matrix phase at the element or micro level, the Tsai-Wu phenomenological failure criterion is used as a basis for comparison to the DMM for the macroscopic failure of the textile composite. Since the Tsai-Wu criterion was formulated in terms of stresses, an adapted form of this criterion in terms of applied force resultants is used:

$$F_{11}N_x^2 + F_{22}N_y^2 + F_{66}N_{xy}^2 + 2F_{12}N_xN_y + F_1N_x + F_2N_y = 1. \tag{18}$$

Employment of this criterion essentially represents fitting an ellipse of Tsai-Wu form to the DMM failure data. The failure coefficients (F_{ij}), which appear in Eq. (18), are based on failure data from the DMM. These parameters are based on the failure strength of the material under various loading conditions, and are typically determined by conducting physical tests on the specimen. For example, in order to obtain F_{11} and F_1, a load of N_x is applied, and all other stresses are set to zero. Then Eq. (18) reduces to:

$$F_{11}N_x^2 + F_1N_x = 1. \tag{19}$$

Since the DMM has been used to determine the maximum uniaxial tensile and compressive force resultant, each of which satisfy Eq. (19), these two independent equations can be solved for F_{11} and F_1:

$$F_1 = (1/X_T) - (1/X_C) \tag{20}$$

$$F_{11} = 1/(X_T - X_C) \tag{21}$$

where X_T and X_C are the failure values of N_x for tension and compression, respectively. Using similar procedures, strength coefficients F_{22}, F_2, and F_{66} are evaluated. The resulting values are as follows:

$$F_2 = (1/Y_T) - (1/Y_C), \tag{22}$$

$$F_{22} = 1/(Y_TY_C), \tag{23}$$

$$F_{66} = 1/s^2. \tag{24}$$

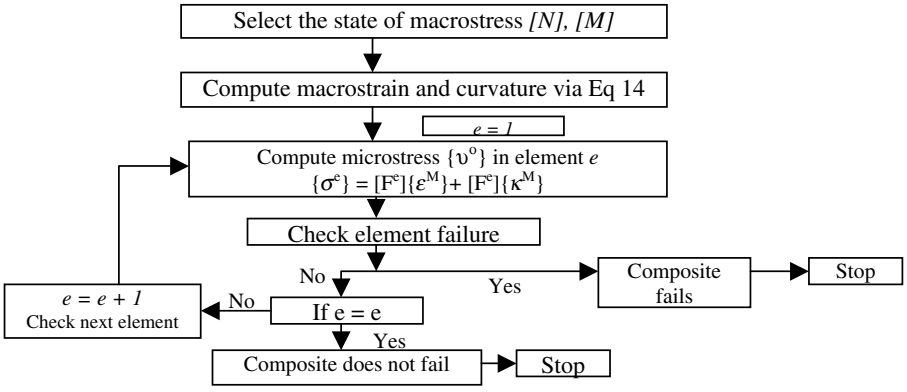

Fig. 3. Flowchart for failure analysis using the direct micromechanics method.

In the above equations Y and S are the strengths in terms of the force resultants N_y and N_{xy}, and C and T denote compression and tension, respectively. In the literature, there exist many proposed methods for determining an appropriate F_{12}. In this paper, the coefficient F_{12} is determined by subjecting the unit-cell to a state of biaxial stress such that $N_x = N_y$ while $N_{xy} = 0$, and then determining the maximum value of applied $N_x = N_y = N_{\max}$. The resulting coefficient takes the following form:

$$F_{12} = \frac{1}{2N_{\max}^2}\left[1 - (F_{11} + F_{22})N_{\max}^2 - (F_1 + F_2)N_{\max}\right]. \tag{25}$$

Please note that for Eqs. (18)–(25), strength values must be in terms of force resultants (N), as noted in the nomenclature. This is different from the textbook definition of the Tsai-Wu failure theory, which is in terms of stresses. Also note that, as will be discussed later, the Tsai-Wu failure theory includes no provision for the incorporation of applied moment resultants into the prediction of failure.

The maximum stress theory is another failure theory to which the results of the DMM may be compared. Simply stated, failure occurs when any single stress component exceeds an allowable level:

$$\begin{aligned} &X_C < N_x < X_T, \\ &Y_C < N_y < Y_T, \\ &|N_{xy}| < S. \end{aligned} \tag{26}$$

And similarly, the maximum strain failure theory states that failure occurs when any single mid-plane strain component exceeds an allowable level:

$$\begin{aligned} &e_C < \varepsilon_{x0} < e_T, \\ &e_C < \varepsilon_{y0} < e_T, \\ &|\gamma_{xy0}| < e_{LT}. \end{aligned} \tag{27}$$

For example, the limiting mid-plane strain in a given direction is:

$$e_i = \frac{N_{\max}/t}{E_i}. \tag{28}$$

The bounds of the maximum strain theory failure envelope take the shape of a parallelogram whose sides are defined by lines of the form:

$$N_y = \nu_{xy} N_x + S_T. \tag{29}$$

As was mentioned regarding the Tsai-Wu failure theory, the maximum stress and maximum strain theories were developed in terms of applied stresses, thus adapted forms of these criteria in terms of applied force resultants are used. Again, currently there is no provision for the incorporation of applied moments into the prediction of failure.

3. Results

3.1. Stiffness properties

The fiber tow was assumed to have material properties of a unidirectional composite (weave geometry is taken into account in the finite element model), in this case AS/3501 graphite–epoxy with the following material properties:

The constitutive matrices relating macroscopic force and moment resultants to strains and curvatures were found using the aforementioned procedures and are found to be:

$$\begin{aligned} [A] &= \begin{bmatrix} 4.14 & 0.52 & 0 \\ 0.52 & 4.14 & 0 \\ 0 & 0 & 0.18 \end{bmatrix} \times 10^6 (Pa - m) \quad [B] \approx 0 \\ [D] &= \begin{bmatrix} 7.70 & 2.53 & 0 \\ 2.53 & 7.70 & 0 \\ 0 & 0 & 1.35 \end{bmatrix} \times 10^{-3} (Pa - m^3) \end{aligned} \tag{30}$$

The character of the constitutive matrices is analogous to an orthotropic stiffness matrix with identical elastic constants in the material principal directions (also referred to as a tetragonal stiffness matrix). Flexural stiffness values of the $[D]$ matrix may seem slightly low, but it should be noted that the RVE under consideration is relatively thin at 0.254 mm. Also note that although the zero terms in the above matrices were not identically zero, they were several orders of magnitude below comparable matrix terms, and thus have been neglected with little or no effect on end results.

The above constitutive matrices have been calculated directly from the micromechanics model without any assumptions on the deformation of the composite such as plane sections remain plane, etc., as in traditional plate theories. The results are quite different from commonly employed approximations. From classical laminate theory, a plane stiffness matrix is calculated from homogenized continuum stiffness properties (i.e., E, G, and ν). The flexural stiffness matrix $[D]$ is then calculated from this homogenized stiffness and the thickness of the textile RVE. By comparison to the direct micromechanics results of the DMM, these methods will misrepresent flexural stiffness values D_{11}, D_{12}, and D_{66} by as much as factors of 2.9, 1.1, and 0.7, respectively. The DMM results imply that there is no consistent relation between in-plane and flexural properties, although the two properties are related.

As a basis for comparison, the following stiffness properties are presented in Table 4, as calculated directly from the $[A]$ and $[D]$ matrices above.

In-plane axial and shear stiffness values (E, G) are calculated directly from the $[A]$ matrix. Compared to the bare properties of the constituent fiber tows (Table 3),

Table 3
Fiber tow and matrix material properties [33]

Material	E_1 (GPa)	E_2 (GPa)	G_{12} (GPa)	ν_{12}
AS/3501 graphite/epoxy (65% fiber volume)	138	9.0	6.9	0.30
3501 Matrix	3.5	3.5	1.3	0.35

Table 4
Stiffness properties for plain weave textile plate

In-plane properties	$E_x = E_y$ (GPa)	G_{xy} (GPa)	ν_{xy}
	16.0	0.71	0.13
Flexural properties	$E_{fx} = E_{fy}$ (GPa)	G_{fxy} (GPa)	ν_{fxy}
	5.0	0.88	0.33

stiffness is lower by an order of magnitude. But it must be noted that the textile composite under consideration here has on overall volume fraction of 25%, whereas the tow properties of Table 3 reflect the 65% volume fraction as seen within the tow itself. Flexural moduli presented in Table 4 are calculated from the following relations:

$$E_{fx} = \frac{-M_x}{I_{yy}\kappa_x} = \frac{12}{t^3 D_{11}}, \tag{31}$$

$$E_{fy} = \frac{12}{t^3 D_{22}}, \tag{32}$$

$$G_{fxy} = \frac{12}{t^3 D_{66}}, \tag{33}$$

$$\nu_{fxy} = \frac{D_{12}}{D_{11}}. \tag{34}$$

Flexural moduli are material-dependent properties, but are strongly geometry-dependent as well. Similarly to what is seen for the in-plane stiffness, the flexural stiffness is shown to be much lower than the constituent tow properties, for the relatively thin plate under consideration here. The bending properties are strongly influenced by the plate thickness and the weave architecture.

3.2. Strength properties

Table 5 shows the textbook values for failure strengths of the yarn and matrix materials. The subscripts "L" and "T" refer to the longitudinal and transverse directions, respectively. The superscripts "+" and "−" refer to tensile and compressive strength. These were used with the Tsai-Wu failure criterion to determine failure of the yarn at the micro level within an element. Note that buckling or instability of the tows is not considered for compressive failure analysis. Though not considered in many textile failure models, its incorporation could be significant given the undulation or waviness of woven tows, and a consequent reduction in allowable compressive stress may be seen [20,21].

Table 5
Fiber tow and matrix failure strength properties (MPa) [33]

	$S_L^{(+)}$	$S_L^{(-)}$	$S_T^{(+)}$	$S_T^{(-)}$	S_{LT}
3501/Graphite tow	1448	1172	48.3	60	62.1
3501 Matrix	70	70	70	70	70

Fig. 4 shows a comparison of the DMM failure envelope for the plain weave graphite/3501 textile composite with several common failure theories: the Tsai-Wu, maximum stress, and maximum strain failure theories. Failure envelopes are shown in the plane of biaxial force resultants with no applied moment present. Since the DMM is used to define the macro level failure strength, all theories share the same uniaxial strengths and are fit to these points. For the most part, the maximum stress theory is much more conservative than all other theories. However, it is less conservative in Quadrants II and IV, since this failure theory does not account for the interaction of biaxial stresses. The maximum strain and Tsai-Wu failure theories compare more closely to the DMM failure envelope, especially the latter.

For zero applied moment (Fig. 4), the DMM failure envelope follows closely with the form of a Tsai-Wu failure envelope. For the most part, the initial failure mode is transverse failure of the fiber tows. However, at the extremes of the major axis of the failure envelope, i.e., the outer corners of quadrants I and III, the initial failure mode transitions to failure of the matrix material. Thus, the DMM failure envelope is cut short at the ends (compared to the failure envelope that would exist if matrix failure were not considered) and is squared-off in these regions and resembles the maximum failure stress (force resultant) criterion. The DMM envelope is more conservative than the Tsai-Wu type criterion in quadrant I, and slightly less conservative in quadrant III. Note that although failure of the bulk matrix may not be considered mechanical failure in some cases, it represents a failure initiation at which point property loss will begin to occur. If needed, without any significant modification, the DMM can be adapted to ignore matrix failure and limit the definition of initial failure to the point at which tow failure is first detected.

Though failure loads are not generally reported in terms of force and moment resultants, a translation of the failure envelope force resultant values to traditional stress values shows that strength magnitudes are reasonable based upon comparison to literature and supplier-reported values for this material, geometry, and the relatively low fiber volume fraction (25%). Since the yarn takes much of the load, the matrix does not begin to fail until a much higher load than its bare tensile strength. Although the strength value is a fraction of the pure tow strength, the woven tow is not completely aligned in the loading directions, i.e., some of the tow is curved into the thickness direction, providing through-thickness reinforcement. Furthermore, after initial transverse failure of

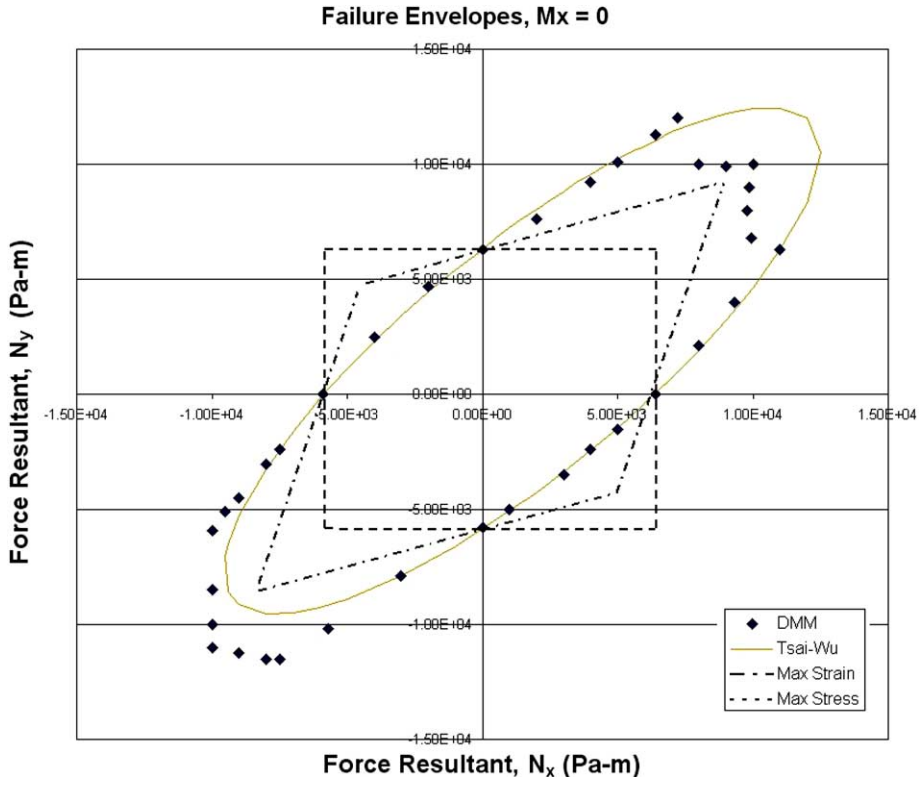

Fig. 4. Comparison of DMM failure envelopes with common failure theories. Adapted forms of the Tsai-Wu, maximum strain, and maximum stress failure theories are shown. Since the DMM is used to define the macro level failure strength, all theories share the same uniaxial strengths and are fit to these points.

the fiber tow (indicative of the introduction of intra-tow micro-cracking), the structure will still maintain load-bearing capacity, though stress concentrations will begin to build up and part integrity will be degraded. Also note that, due to symmetry of the textile RVE about the x- and y- axes, the failure envelope exhibits this symmetry as well.

The effect of an added moment M_x on the failure envelope is shown in Fig. 5 with the applied moment M_x equal to half the critical value that would cause failure if it were the only applied load. The figure also includes results from Fig. 4, the DMM results and quadratic failure envelope for the case of zero applied bending moment. There is no Tsai-Wu, maximum stress, or maximum strain failure envelope to include applied moment resultants, as these theories are not developed to include such load types. As has been mentioned, strength estimates will be somewhat conservative given that failure is defined as failure of a single element that surpasses the maximum allowable microstress, but this presents a realistic definition of initial failure.

Continuing to inspect Fig. 5, an applied moment in the x-direction has the expectable effect of shrinking the failure envelope in regions where tensile applied loads dominate. However, when only compressive loads are applied, an applied moment can actually increase the in-plane load capacity by offsetting some of the compressive stress with bending-induced tension. The magnitude of this load-capacity increase is limited, however, by the eventual failure of the matrix. As with the case of pure in-plane loading, the failure envelope at the outer corner of quadrant III is dominated by matrix failure. The effects of applied moment on the failure envelope of the plain weave textile represents the importance of the consideration of stress gradients, or load non-uniformities. The appreciable difference that arises suggests that such consideration could be critical to the successful design or optimization of a textile structural component.

The effect of changing the failure theory used to define failure of a tow element at the micro (elemental) level is shown in Fig. 6. The DMM can easily be modified to employ any appropriate failure criterion for the constituent phases at the micromechanical level. Here, the maximum stress failure theory (MSFT) is used to replace the Tsai-Wu failure theory to determine first-element failure for the fiber tows. Though the overall character of the failure envelope is unchanged, the effect is significant in that the failure envelope becomes roughly half as conservative. So although the size of the failure envelope is a function

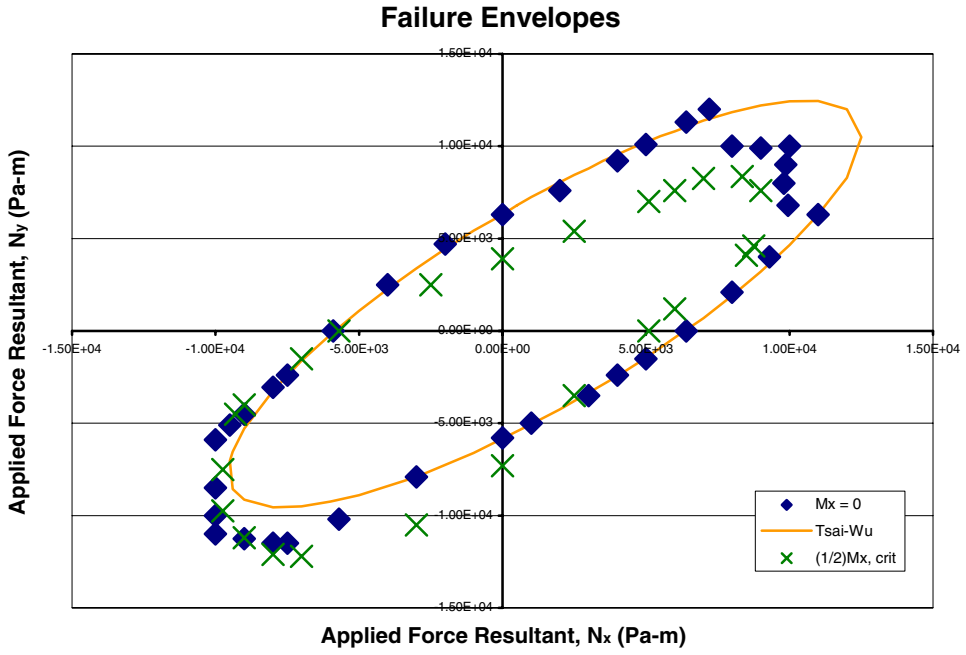

Fig. 5. Effect of bending moment on the failure envelope. The orientation of the axes of the failure ellipse seem to rotate, and the overall envelope decreases in size. The Tsai-Wu failure ellipse is unaltered when moment is applied, as the theory includes no provision for this load type.

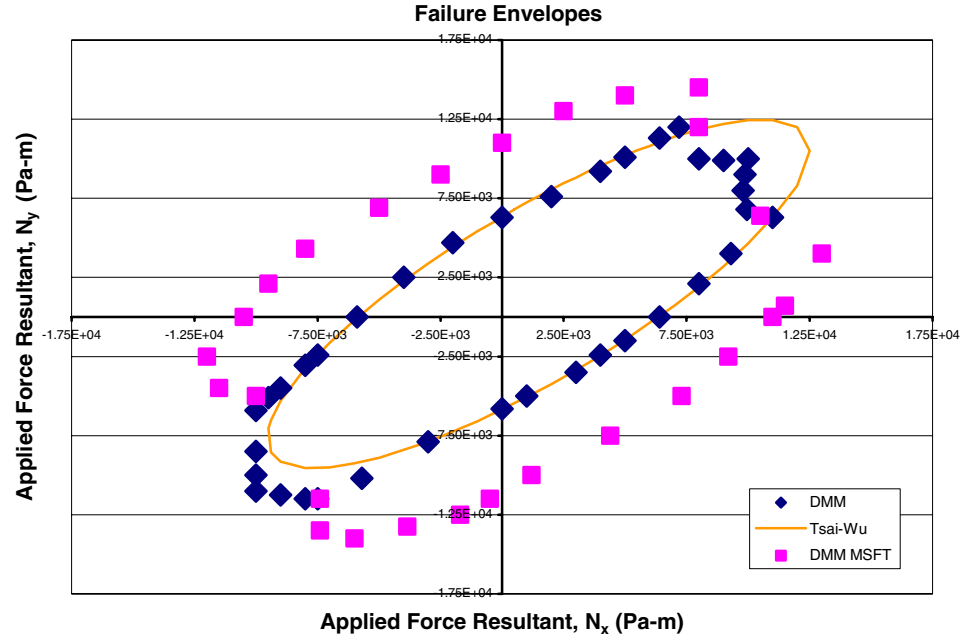

Fig. 6. Effect of micro-level tow failure theory on the DMM failure envelope. A comparison is shown between the original DMM using the Tsai-Wu theory to analyze failure of a two element and an altered DMM in which the MSFT is used.

of the choice of these two quite different failure theories, the character of the failure envelope does not seem to be an artifact of the choice of micro-level failure criterion. It should be noted that, even in the case of simple uniaxial macro applied loads, the micro stress field that results is fully three-dimensional and non-homogeneous across the RVE. Thus, especially for the orthotropic fiber tows, a failure theory that includes multi-dimensional stress interaction effects (such as Tsai-Wu) should be more appropriate.

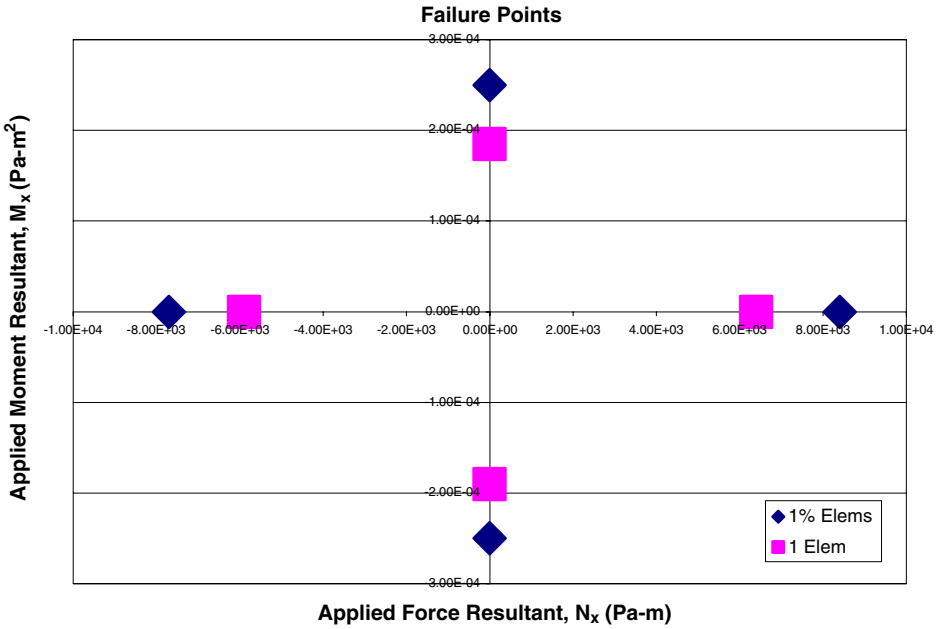

Fig. 7. Effect of changing the definition of micro-level failure point on the failure envelope. The critical applied force or applied moment needed to initiate failure is shown to increase by roughly 30% if failure is defined as the point at which 1% of elements have exceeded failure criterion, rather than the point at which 1 single element has failed.

As mentioned earlier we have assumed that the entire textile composite has failed, even if only one of the yarn or matrix elements has failed. This is very conservative. In fact we can change the definition of failure by stating that failure is considered to have occurred when 1% of the total number of elements in the model have failed. Fig. 7 shows the effect of changing the definition of failure in the textile composite and consequently the macro failure envelope. Note that the axes are different from previous failure plots, in order to illustrate these effects under different loading types. Failure points are shown in the plane of uniaxial applied force and moment resultants. About 30% increase in maximum allowable force or moment resultant results from changing the definition of initial failure. This is shown to present the possibility of a more stochastic or a less conservative approach to determining the point at which initial failure occurs. Thus, only a few points are presented to show the relative magnitude of the force or moment needed to cause failure under the two failure definitions.

3.3. Micro stress field contour plots

Detailed stress-field contour plots are one output of the DMM that provide great insight into the failure modes and points of maximum stress in the RVE. Tow or matrix portions of the RVE can be isolated for individual scrutiny. Fig. 8 shows the stress field for the plain-weave fiber tows in uniaxial tension. Most of the load in this case is taken by the fiber tows aligned in the loading direction. However, the failure mode is transverse failure of the cross-axis tows, as the strength is much lower in this direction. Tows aligned in the direction of loading tend to be pulled straight as load is applied. This has the secondary effect of applying bending to the cross-axis tows, creating significant bending stresses. The maximum stress levels in this micro stress field tend to occur around the matrix pockets between tows, which tend to act as a micromechanical stress concentration. Similar inspection of the stress field in the matrix surrounding the fiber tows (not shown here) shows that the maximum stress tends to occur along the relatively sharp edges of the lenticular fiber tows, which again tend to act as a micromechanical geometrical stress concentration.

Further stress contour plots illustrating results and capabilities of the DMM show the RVE behavior in shear and bending load cases. For unit bending load cases, it is shown that the majority of the load is again taken by the fiber tows along the direction of curvature. Furthermore, just as there is a transition from tension to compression across the RVE in bending, a rapid stress gradient from tension to compression can be seen in an individual fiber tow. This again suggests the importance of the consideration of stress gradients in the micromechanical characterization of a textile RVE.

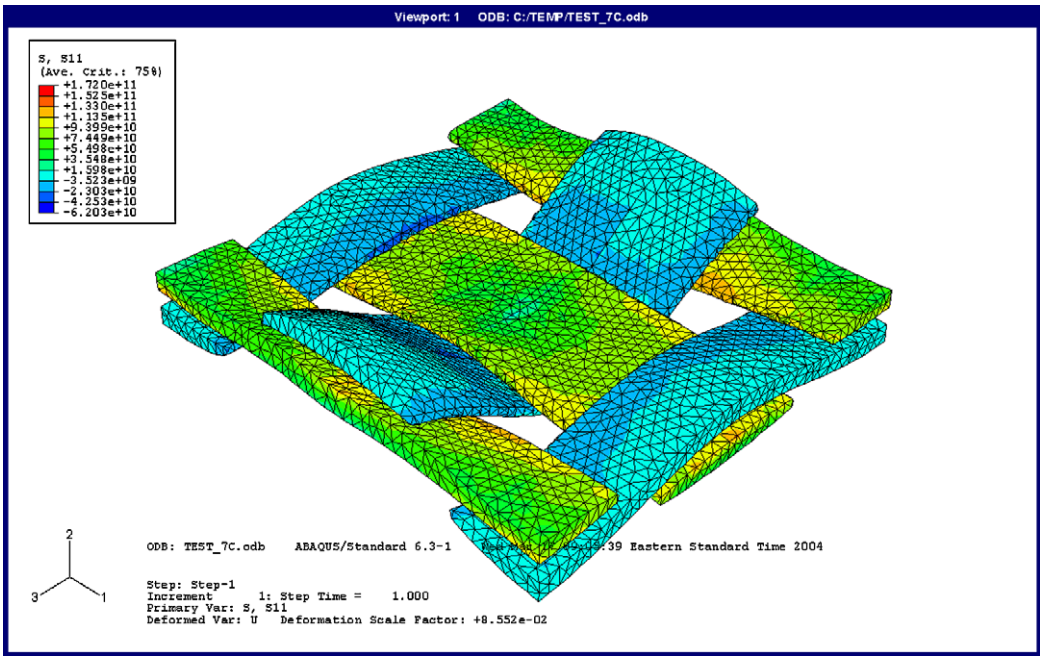

Fig. 8. Stress contours for plain-weave fiber tows in uniaxial extension. Detailed microstress field results from the DMM provide valuable insight into the mechanical response of an RVE under any loading condition. Tow elements or matrix elements can be isolated to provide further detail.

4. Conclusions

By analysis of the microstresses developed in a representative volume element (RVE), the direct micromechanics method (DMM) has been used to construct failure envelopes for a plain weave carbon/epoxy textile composite in plane stress. To allow for the accommodation of stress gradients, or non-uniform applied loads, micromechanical analysis had been performed in terms of classical laminate theory force and moment resultants $[N]$, $[M]$ and constitutive matrices $[A]$, $[B]$, $[D]$. The predicted values of the stiffness matrices and ultimate strength values compare well to expectable magnitudes. The DMM failure envelope was shown to be largely elliptical of the form of a Tsai-Wu failure criterion and dominated by transverse fiber tow failure. But in cases of large biaxial tension or biaxial compression loads, the DMM failure envelope compared to the form of the maximum stress criterion, and matrix failure was the mode of initial failure. The presence of applied moment resultants $[M]$, as would exist in cases of non-uniform load across the RVE, was shown to have a significant effect on the failure envelope. Thus its consideration, not covered in conventional failure models, can be critical.

Acknowledgements

This work was performed under Army Research Office contract DAAD19-02-1-0330 with Dr. Bruce LaMattina as the Grant Monitor. This support is gratefully acknowledged. The authors are thankful to Dr. Jerome Tzeng, Army research laboratories at Aberdeen Proving Grounds for many helpful discussions.

References

[1] Tsai SW, Hahn HT. Introduction to composite materials. Lancaster (PA): Technomic Publishing Co; 1980.
[2] Dasgupta AS, Bhandarkar S, Pecht M, Barkar D. Thermoelastic properties of woven-fabric composites using homogenization techniques. In: Proceedings of the American society for composites, fifth technical conference, Lansing, MI; 1990. p. 1001–10.
[3] Foye RI. Approximating the stress field within the unit cell of a fabric reinforced composite using replacement elements. NASA CR-191422; 1993.
[4] Naik RA. Analysis of woven and braided fabric reinforced composites. NASA CR-194930; 1994.
[5] Whitcomb JD. Three-dimensional stress analysis of plain weave composites. Composite materials fatigue and fracture (third volume), ASTM STP 1110; 1991. p. 417–38.
[6] Ishikawa T, Chou TW. One-dimensional micromechanical analysis of woven fabric composites. AIAA J 1983;21:1714–21.
[7] Ma CL, Yang JM, Chou TW. Elastic stiffness of three-dimensional braided textile structural composites. Composite materials: testing and design (7th conference), ASTM STP 893; 1986. p. 404–21.
[8] Raju IS, Foye RL, Avva VS. A review of analytical methods for fabric and textile composites. In: Proceedings of the Indo-US workshop on composite materials for aerospace applications, Bangalore, India, Part I; 1990. p. 129–59.
[9] Whitcomb JK, Srirengan K. Effect of various approximations on predicted progressive failure in plain weave composites. Compos Struct 1996;34:13–20.
[10] Lomov SE et al. Textile composites: modelling strategies. Composites: Part A 2001;32:1379–94.

[11] Hochard C, Aubourg PA, Charles JP. Modelling of the mechanical behavior of woven-fabric CFRP laminates up to failure. Compos Sci Technol 2001;61:221–30.
[12] Huang ZM, Ramakrishna S. Modeling inelastic and strength properties of textile laminates: a unified approach. Compos Sci Technol 2002;63:445–66.
[13] Bigaud D, Hamelin P. Stiffness and failure modelling of 2D and 3D textile reinforced composites by means of imbricate type elements approaches. Comput Struct 2002;80:2253–64.
[14] Woo K, Whitcomb JD. A post processor approach for stress analysis of woven textile composites. Compos Sci Technol 2000;60:693–704.
[15] Tang X, Whitcomb JD. General techniques for exploiting periodicity and symmetries in micromechanics analysis of textile composites. J Compos Mater 2003;37:13.
[16] Cox BN, Dadkhah MS. A binary model of textile composites: I – formulation. Acta Metall Mater 1994;42(10):3463.
[17] Yang Q, Cox BN. Predicting local strains in textile composites using the binary model formulation. In: Proceedings of the ICCM 2003, San Diego, CA, July; 2003.
[18] Bogdanovich AE, Pastore CM. Material-smart analysis of textile-reinforced structures. Compos Sci Technol 1996;56:291–309.
[19] Bogdanovich AE. Multiscale predictive analysis of 3-D woven composites. In: SAMPE 35th international technical conference, CD ROM proceedings, Dayton, OH; September 2003.
[20] Quek SC, Waas A, et al. Compressive response and failure of braided textile composites: Part 2 – computations. Int J Nonlinear Mech 2004;39:649–63.
[21] Quek SC, Waas A, et al. Compressive response and failure of braided textile composites: Part 1 – experiments. Int J Nonlinear Mech 2004;39:635–48.
[22] Cox BN, Dadkhah MS, Morris WL. Failure mechanisms of 3D woven composites in tension, compression, and bending. Acta Metall Mater 1994;42(12):3967–84.
[23] Pochiraju K, Chou TW, Shah BM. Modeling stiffness and strength of 3D textile structural composites. In: Proceedings of the 37th joint AIAA/ASME/ASCE/AMS/ASC structures, structural dynamics, and materials conference, Salt Lake City, UT; 1996.
[24] Dadhkah MS, Morris WL, Kniveton T, Cox BN. Simple models for triaxially braided composites. Composites 1995;26:91–102.
[25] Fleck NA, Jelf PM. Deformation and failure of a carbon fiber composite under combined shear and transverse loading. Acta Metall Mater 1995;43(8):3001–7.
[26] Swanson SR, Smith LV. Multiaxial stiffness and strength characterization of 2D braid carbon/epoxy fiber composites. In: Poe CC, editor. Mechanics of textile composites conference, Hampton, VA. NASA Conference Publication 3311; 1995.
[27] Sankar BV, Lee BW, Karkkainen RL. Evaluation of failure criteria for plain weave textile composites using finite element micromechanics. In: Proceedings of the 35th international SAMPE technical conference, Dayton, OH; September 2003.
[28] Zhu H, Sankar BV, Marrey RV. Evaluation of failure criteria for fiber composites using finite element micromechanics. J Compos Mater 1998;32(8):766–82.
[29] Marrey RV, Sankar BV. Micromechanical models for textile structural composites. NASA CR-198229; 1995.
[30] Sankar BV, Marrey RV. Analytical method for micromechanics of textile composites. Compos Sci Technol 1997;57(6):703–13.
[31] Marrey RV, Sankar BV. A micromechanical model for textile composite plates. J Compos Mater 1997;31(12):1187–213.
[32] Carvelli V, Poggi C. A homogenization procedure for the numerical analysis of woven fabric composites. Compos Part A: Appl Sci Manuf 2001;32:1425–32.
[33] Gibson RF. Principles of composite material mechanics. New York: McGraw-Hill, Inc.; 1994.